AIAA JOURNAL
Vol. 42, No. 11, November 2004

Scramjet Inlet Control by Off-Body Energy Addition: A Virtual Cowl

Sergey O. Macheret,* Mikhail N. Shneider,† and Richard B. Miles‡
Princeton University, Princeton, New Jersey 08544

The theory of energy addition to hypersonic airflow off the vehicle to increase air mass capture and reduce spillage in scramjet inlets at Mach numbers below the design value is explored. The heated region creates a virtual cowl and deflects flow streamlines into the inlet. Optimization studies are performed with a two-dimensional inviscid fluid code. The best location of the energy addition region is near the intersection of the nose shock of the vehicle with the continuation of the cowl line, and slightly below that line. In that case, the shock generated by the heating is close to the shock that is a reflection of the vehicle nose shock off the imaginary solid surface-extension of the cowl. Effects of the size and shape of the energy addition region on inlet performance are also studied.

I. Introduction

THE optimum geometry of scramjet-powered hypersonic vehicles corresponds to the well-known shock-on-lip (SOL) condition (Fig. 1): The compression ramp shocks converge on the cowl lip, and the reflected shock impinges on the shoulder of the inlet.[1] Because shock angles are determined by the flight mach number, the SOL condition cannot be met at mach numbers higher or lower than the design mach number.[1] Typically, inlets are designed for the highest Mach number expected in the hypersonic airbreathing flight, and at Mach numbers lower than the design value, the so-called spillage occurs and the air mass capture decreases (Fig. 2).

To avoid performance penalties at off-design Mach numbers, a variable geometry inlet can be used. However, the mechanical variable geometry system would be quite heavy. An alternative approach is to optimize inlets using energy addition to or extraction from the flow. Plasmas and various magnetohydrodynamic devices may offer viable flow control and inlet optimization schemes.[2–8]

In the present paper, we analyze a new concept of increasing the mass capture, suggested recently in Ref. 2 and dubbed a virtual cowl. The essence of the method is to create a heated region upstream of and somewhat below the cowl lip (Fig. 3). The incoming flow would be deflected by the elevated-temperature and/or elevated-pressure region, causing an increased mass flow into the inlet. The mechanism of energy addition is unspecified. For example, the heated region may be generated by supplying microwave or rf energy to a volume preionized by a focused laser or electron beam. Other possible means include plasma or hot-air jets and external combustion. Shooting combustible liquid or solid pellets[9] may be an interesting option. An important advantage of the new method is that the air entering the inlet would have experienced little or no heating. Thus, irreversibilities and stagnation pressure losses associated with heating can be minimized.

The purpose of this paper is to study computationally the virtual cowl concept and to determine optimum location and shape of the heat addition region, without specifying the energy addition mechanism.

II. Model and Computational Procedure

We consider hypersonic gas flow along a series of compression ramps upstream of the inlet with forward-shifted cowl lip, as schematically shown in Figs. 1–3. The flow is two dimensional in the (x, z) plane, where x is the freestream flow direction and z is directed from the vehicle nose downward. Cases both without and with heat addition are computed with the set of Euler equations together with perfect gas equation of state. Because the entire flow region is supersonic, a steady-state solution using x as a marching coordinate can be found. The heat addition rate profile is Gaussian, that is, it is proportional to $\exp[-(x-x_0)^2/r_{\text{eff},x}^2 - (z-z_0)^2/r_{\text{eff},z}^2]$, where x_0 and z_0 are coordinates of the center of the heating region and $r_{\text{eff},x}$ and $r_{\text{eff},z}$ are the effective radii. The parameters x_0, z_0, $r_{\text{eff},x}$, and $r_{\text{eff},z}$ are varied in computations to find optimal values of these parameters. In circular-cylinder Gaussian cases, $r_{\text{eff},x} = r_{\text{eff},z} = r_{\text{eff}}$. In elliptical-cylinder Gaussian cases, $r_{\text{eff},x} \neq r_{\text{eff},z}$, the heating profile may also be tilted at an angle α_q with respect to the x axis.

The inlet performance is characterized by the total enthalpy entering the inlet throat per second per unit length in the spanwise direction, $\dot{H}$, the average Mach number at the throat, M, the mass capture coefficient k_m, the ratios of stagnation pressure and static pressure, density, and temperature at the throat to their freestream values (k_{p_t}, k_p, k_ρ, and k_T), and adiabatic and cooled kinetic energy efficiencies, $\eta_{\text{KE,ad}}$ and $\eta_{\text{KE,cool}}$.

In many cases, the flow at the inlet throat is quite nonuniform and not parallel to the walls. Therefore, a proper procedure of averaging flow parameters at the throat has to be employed. In this work, we use the so-called stream-thrust averaging commonly accepted in inlet design.[1] This procedure, described in Ref. 1, effectively takes into account losses of total pressure (entropy increase) that would occur downstream of the throat, in the isolator, when the flow is allowed to settle and to become parallel to the walls.

III. Computed Cases

Freestream conditions in all computed cases corresponded to flight at Mach 6, 8, or 10, with dynamic pressure of either 1000 psf (47,880.25 Pa) or 2000 psf (95,760.5 Pa). The freestream parameters are listed in Table 1. The baseline case was that of Mach 10 flight with 0-deg angle of attack. The three-ramp inlet (2.5-, 8.0-, and 11.0-deg ramp angles) was chosen so that the nose shock would barely (by about 1 in.) miss the cowl lip and the flow would be almost parallel to the isolator walls downstream of the inlet throat. This design geometry, as well as the shock pattern at Mach 6, with flow spillage, is shown in Fig. 4. Figure 5 shows static temperature contours and flow streamlines at Mach 6, 2000 psf, demonstrating

Presented as Paper 2003-0032 at the AIAA 41st Aerospace Sciences Meeting, Reno, NV, 6–9 January 2003; received 20 July 2003; revision received 2 May 2004; accepted for publication 1 June 2004.

*Senior Research Scientist, Department of Mechanical and Aerospace Engineering, D-414 Engineering Quadrangle; macheret@princeton.edu. Associate Fellow AIAA.

†Research Staff Member, Department of Mechanical and Aerospace Engineering, D-414 Engineering Quadrangle. Member AIAA.

‡Professor, Department of Mechanical and Aerospace Engineering, D-414 Engineering Quadrangle. Fellow AIAA.

Table 1 Freestream parameters[a]

Mach	h, km	p_0, Pa	T_0, K
6	26.93/22.47	1900/3800	223.47/218.98
8	30.76/26.155	1068.75/2137.5	227.26/222.70
10	33.789/29.108	684/1368	233.16/225.63

[a]Altitude h and static pressure and temperature, p_0 and T_0, in computed cases with flight dynamic pressure of $q = 1000/2000$ psf.

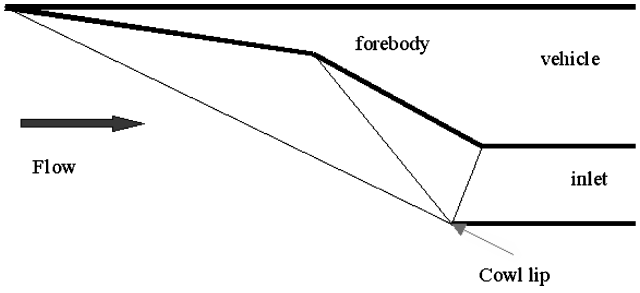

Fig. 1 Design forebody and inlet geometry with SOL condition.

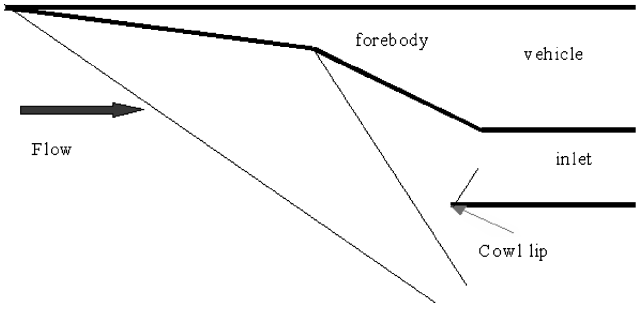

Fig. 2 Shock geometry at Mach number lower than the design value, with flow spillage.

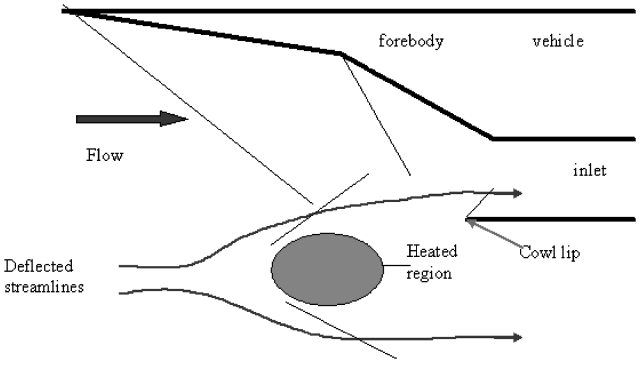

Fig. 3 Schematic diagram of virtual cowl concept: off-body heat addition increases mass capture.

the spillage. The vertical arrow in Fig. 5, and where shown subsequently, indicates the position of inlet throat.

To reduce the spillage, the cowl might be extended upstream, as shown in Fig. 6, although this can be difficult to accomplish practically. However, the case with extended solid cowl can serve as a guide to optimizing virtual cowl cases. Qualitatively, one would expect that the virtual cowl, that is, off-body energy addition, should, for the best performance, create a flow pattern imitating that of the solid extended cowl. Because shocks do not reflect off a heated region, the analogy between the solid and virtual cowls is not exact. However, the heated region can generate a shock wave that would mimic the shock reflected from the solid surface on incidence of the nose shock on it. Thus, one would expect that the energy addition should be more or less concentrated and that it should be

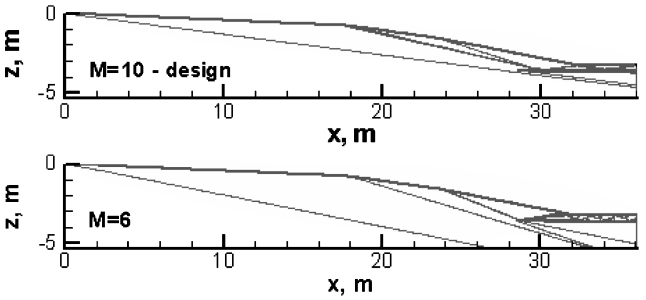

Fig. 4 Shock patterns (Mach number contours) at the design Mach 10 and off-design Mach 8 and 6 cases.

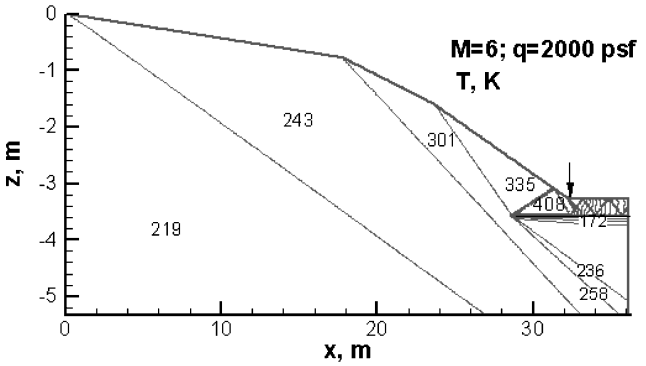

a)

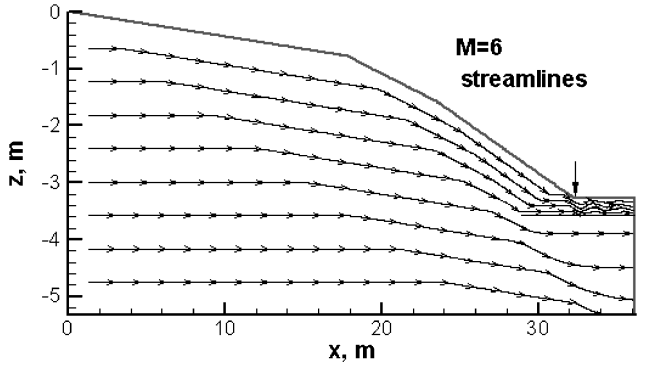

b)

Fig. 5 Mach 6, 2000-psf case without energy addition: a) static temperature and b) flow streamlines.

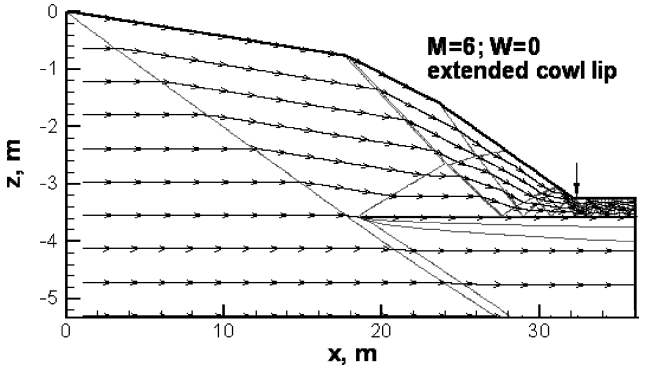

Fig. 6 Shock pattern and flow streamlines at Mach 6 with an extended solid cowl.

Table 2 Inlet performance parameters in optimum virtual cowl cases at 1000 psf of dynamic pressure

Energy addition rate, MW/m	k_m	k_{p_t}	k_p	k_ρ	k_T	M	$\eta_{\mathrm{KE,ad}}$	η_{KE}	$\dot{H}$, MW/m
				$M = 10$					
	0.955	0.6147	41.26	12.4	3.32	5.15	0.992	0.992	523.26
				$M = 8$					
$W = 0$	0.889	0.628	38.86	11.96	3.25	4.03	0.989	0.989	395.0
$W = 0$, ext CL	0.98	0.701	42.538	13.165	3.23	4.04	0.991	0.991	435.3
$W = 5$	0.952	0.695	40.938	12.77	3.2	4.06	0.991	0.991	423.0
$W = 10$	0.99	0.689	43.561	13.31	3.27	4.01	0.991	0.991	439.8
				$M = 6$					
$W = 0$	0.731	0.67	31.6	10.51	3.0	2.94	0.983	0.983	255.2
$W = 0$, ext CL	0.981	0.82	44.78	14.28	3.135	2.84	0.992	0.992	342.4
$W = 5$	0.788	0.73	33.85	11.31	2.99	2.95	0.987	0.987	275.0
$W = 10$	0.833	0.677	33.68	12.18	3.175	2.81	0.983	0.983	290.8
$W = 2 \times 2.5$	0.79	0.734	33.86	11.33	2.987	2.95	0.987	0.987	275.6
$W = 2 \times 5$	0.833	0.763	36.03	11.97	3.0	2.93	0.988	0.988	290.7
$W = 35$ $x_Q = 18.5$ m $z_{\mathrm{CL}} - z_Q = 1.3$ m	0.983	0.633	52.73	14.9	3.53	2.56	0.980	0.980	342.9
$W = 20$ $x_Q = 7.5$ m $z_{\mathrm{CL}} - z_Q = 4$ m	0.904	0.818	39.34	13.01	3.02	2.92	0.992	0.992	315.4

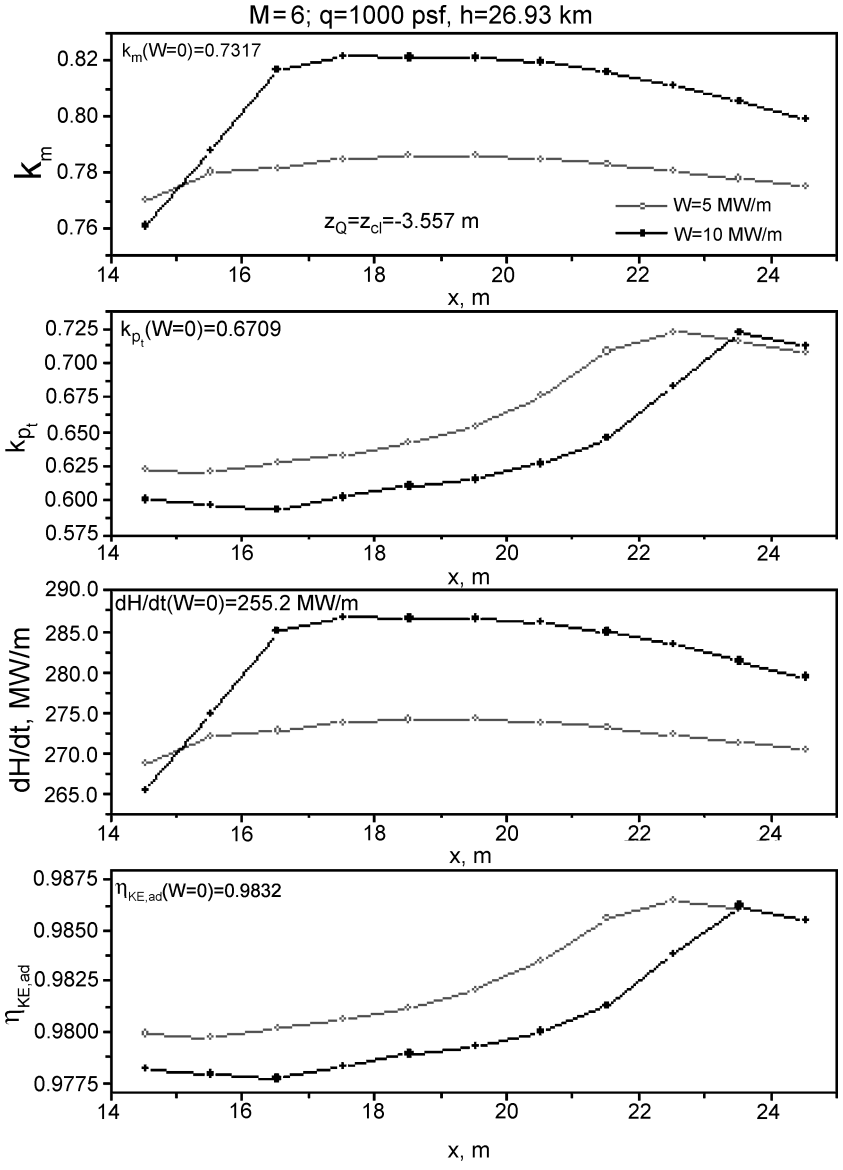

Fig. 7 Inlet performance parameters at Mach 6, 1000 psf, vs streamwise distance of the energy addition region from the vehicle nose, at two values of energy addition rate W, center of energy addition fixed at cowl level z_{cl}.

Table 3 Variation of computed inlet parameters with grid size[a]

Power deposition, MW/m	k_m	k_{p_t}	k_p	k_ρ	k_T	M	$\eta_{\mathrm{KE,ad}}$	η_{KE}	$\dot{H}$, MW/m
$W=0$	0.731[b]	0.67	31.6	10.51	3.0	2.94	0.983	0.983	255.2
	(0.726)[c]	(0.677)	(31.01)	(10.4)	(2.98)	(2.96)	(0.983)	(0.983)	(253.3)
$W=5$	0.788	0.73	33.85	11.31	2.99	2.95	0.987	0.987	275.0
	(0.783)	(0.735)	(33.38)	(11.22)	(2.97)	(2.96)	(0.987)	(0.987)	(273.4)

[a]Mach 6, 1000-psf cases without energy addition ($W=0$) and with optimally located energy addition source of $W=5$ MW/m.
[b]Obtained with $12{,}500 \times 240$ grid.
[c]Obtained with 6250×120 grid.

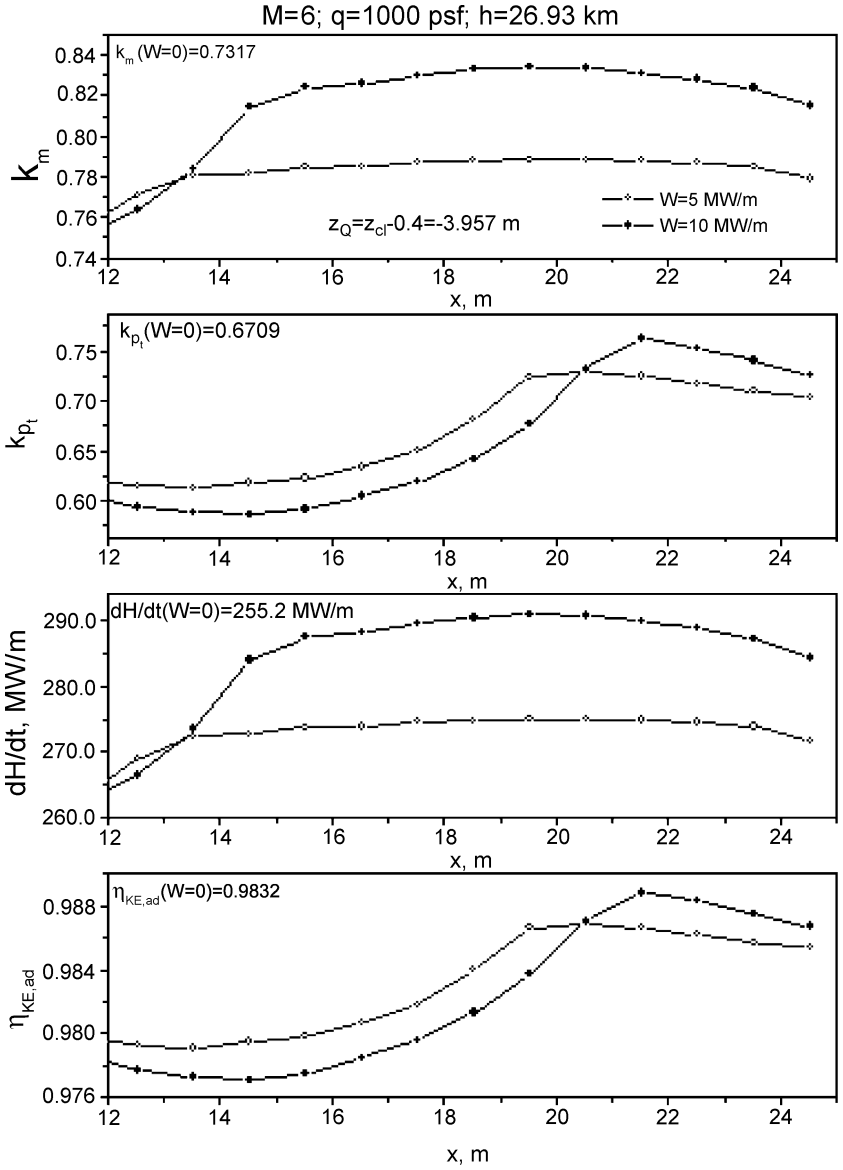

Fig. 8 Inlet performance parameters at Mach 6, 1000 psf, vs streamwise distance of the energy addition region from the vehicle nose, at two values of energy addition rate W, center of energy addition fixed at 0.4 m below cowl level z_{cl}.

positioned near the intersection of the nose shock with the upstream continuation of the cowl.

Note that heating and the resulting expansion of the gas would adversely affect both mass flow rate and stagnation pressure at the throat if the heated air is allowed to enter the inlet. Therefore, the energy addition region should be shifted somewhat down, so that heated and expanded air would miss the inlet, whereas cold air would be compressed and deflected into the inlet.

The qualitative expectations of the preceding two paragraphs were confirmed in calculations, as shown in Figs. 7 and 8 for Mach 6, 1000-psf, zero-angle-of-attack flight. In these calculations, circular-cylinder Gaussian heat addition, with $r_{\mathrm{eff},x} = r_{\mathrm{eff},z} = r_{\mathrm{eff}} = 0.2$ m was assumed. (This value of r_{eff} was found to be close to the optimum, to be discussed.) In both Figs. 7 and 8, the values of performance parameters in the absence of energy addition ($W=0$) are indicated in the upper left-hand corners. In Fig. 7, the vertical location of the

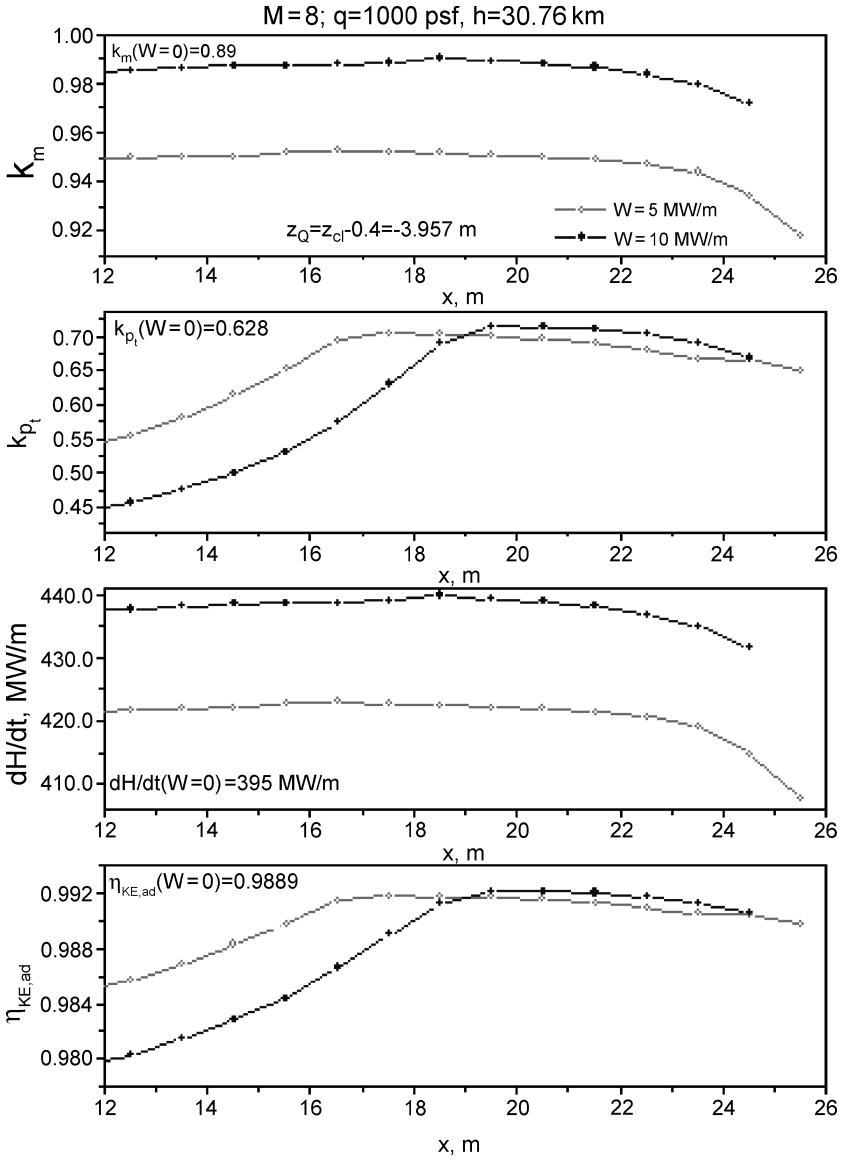

Fig. 9 Inlet performance parameters at Mach 8, 2000 psf, vs streamwise distance of energy addition region from vehicle nose, at two values of energy addition rate W.

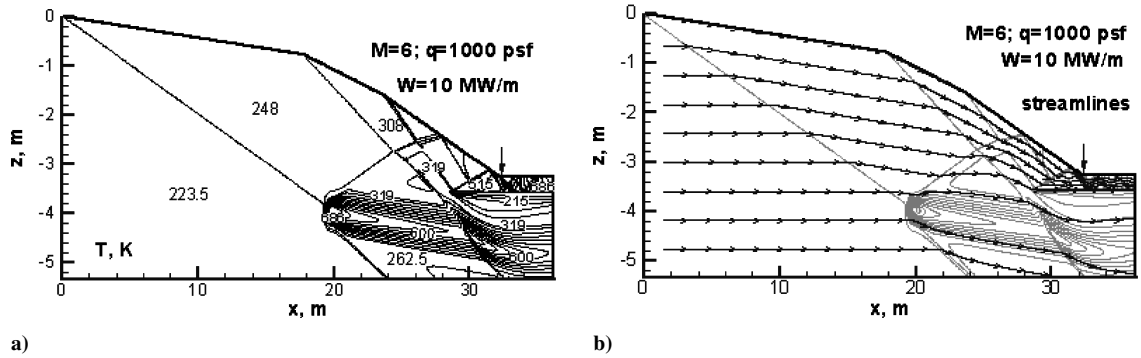

a) b)

Fig. 10 Mach 6, 1000 psf, with optimum location of circular Gaussian virtual cowl with $r_{\text{eff}} = 0.2$ m, and $W = 10$ MW/m: a) static temperature contour lines and b) flow streamlines.

center of energy addition region was fixed at the cowl level, $z_Q = z_{\text{cl}}$, and in Fig. 8 the vertical location of the energy addition was shifted down by $2r_{\text{eff}} = 0.4$ m. In both Figs. 7 and 8, key inlet performance parameters are plotted vs horizontal coordinate of the energy addition center, at two values of the integral energy addition rate, W. As seen in Figs. 7 and 8, energy addition does increase the mass capture, and the effect becomes stronger as more energy is added. Mass capture and the enthalpy flux both exhibit broad maxima at the value of x approximately corresponding to the intersection of the nose shock with the upstream continuation of the cowl. Total pressure and adiabatic kinetic energy coefficients also have their peaks, but at a value of x somewhat shifted downstream with respect to that where mass capture is maximum. However, because the maximum of mass capture is very broad, a location maximizing both k_m and k_{p_i} can be reasonably selected. As predicted in the preceding paragraph, shifting the center of energy addition region down from the cowl line

Table 4 Inlet performance parameters at Mach 6, 1000 psf, without heat addition ($W = 0$), with extended solid cowl ($W = 0$, ext CL), and with optimally located $W = 10$ MW/m heating source with different effective radii $r_{\text{eff},x}$ and $r_{\text{eff},z}$ and tilt angle α_q

Case	k_m	k_{p_t}	k_p	k_ρ	k_T	M	$\eta_{\text{KE,ad}}$	η_{KE}	$\dot{H}$, MW/m
$W = 0$	0.731	0.67	31.6	10.51	3.0	2.94	0.983	0.983	255.2
$W = 0$, ext CL	0.981	0.82	44.78	14.28	3.135	2.84	0.992	0.992	342.4
$W = 10$ MW/m; $r_{\text{eff},x} = 0.2$ m $r_{\text{eff},z} = 0.2$ m	0.833	0.677	33.68	12.18	3.175	2.81	0.983	0.983	290.8
$W = 10$ MW/m; $r_{\text{eff},x} = 3$ m $r_{\text{eff},z} = 0.2$ m $\alpha_q = 0$	0.839	0.760	36.53	12.08	3.02	2.926	0.988	0.988	292.9
$W = 10$ MW/m; $r_{\text{eff},x} = 3$ m $r_{\text{eff},z} = 0.2$ m $\alpha_q = 2.5^0$	0.844	0.728	37.8	12.23	3.09	2.875	0.986	0.986	294.5

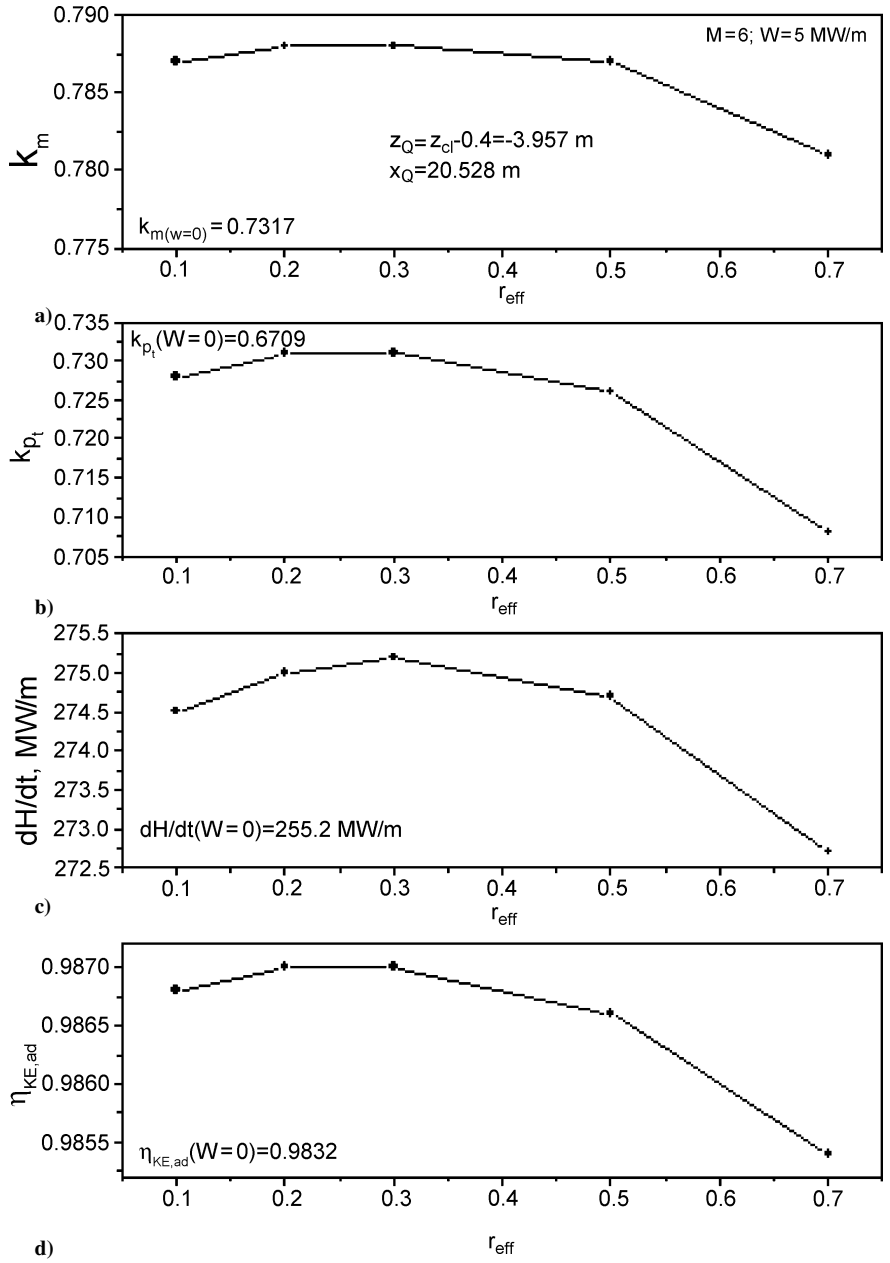

Fig. 11 Variation of inlet performance parameters with the effective radius of circular Gaussian energy addition region.

somewhat improves inlet performance; indeed, maximum values of both k_m and k_{p_i} are greater in Fig. 8 than they are in Fig. 7. (Note that, in calculations not shown here, we found that shift by $2r_{\text{eff}} = 0.4$ m is near optimal because moving the energy addition center farther downward decreases the performance.) At other Mach numbers and dynamic pressures, the behavior is similar to that shown in Figs. 7 and 8. For example, Fig. 9 shows the Mach 8, 1000-psf case with energy addition center shifted down by $2r_{\text{eff}} = 0.4$ m. The energy addition profile is circular Gaussian with $r_{\text{eff}} = 0.2$ m, and the vertical location z_Q of the center of energy addition is fixed at 0.4 m below the cowl level z_{cl}. The values of performance parameters in the absence of energy addition ($W = 0$) are indicated in the upper left-hand side. The maxima of inlet performance parameters here are even broader with respect to x than they are in Figs. 7 and 8. Static temperature contours and flow streamlines in the Mach 6, 1000-psf case with energy addition rate of $W = 10$ MW/m centered near the optimum location (Fig. 8) are shown in Fig. 10, where the shock and flow patterns are seen to imitate those of the extended solid cowl case of Fig. 6.

Next, placing the center of energy addition region in its optimum location and varying the effective radius r_{eff}, the optimum value of r_{eff} was found. As shown in Fig. 11, inlet performance coefficients have very broad maxima in the vicinity of $r_{\text{eff}} = 0.2 - 0.3$ m, which justifies the selection of $r_{\text{eff}} = 0.2$ m in optimization studies of energy addition location. The values of performance parameters without energy addition, $W = 0$, are also shown. The center of energy addition region is at its optimum location (x_Q, z_Q) indicated in Fig. 11a. Total deposited power is $W = 5$ MW/m. Freestream flow conditions are Mach 6 and 1000 psf.

The next issue addressed in our analysis was how inlet performance would be affected if, instead of a single energy addition region, two energy addition regions are used with the total power equal to that of the single region. Figure 12 shows such a case, at Mach 6, 1000 psf, with two sources of 2.5 MW/m each. We found that, with proper positioning of the second source downstream of the first one, the inlet performance would not decrease compared with that given by a single of 5 MW/m. The same conclusion was reached at other Mach numbers, dynamic pressures, and total power levels.

Table 2 lists the inlet performance parameters in all optimum cases at 1000 psf of dynamic pressure, with circular-cylinder Gaussian heating profile ($r_{\text{eff}} = 0.2$ m). Two cases with $W = 20$ and 35 correspond to heating source location (x_Q, z_Q) substantially below the cowl line z_{CL}; in other energy addition cases, the source is located just below the cowl level. For comparison, cases with no heat addition ($W = 0$) and with extended solid cowl (ext CL) are also shown. As seen in Table 2, at Mach 8, virtual cowl with 10 MW/m energy addition rate can match the performance of the extended solid cowl in terms of both mass capture k_m and kinetic energy efficiency η_{KE}, and this performance is substantially higher than without extended or virtual cowls. At Mach 6, with spillage substantially greater than that at Mach 8, energy addition of $W = 10$ MW/m yields the mass capture k_m and the kinetic energy efficiency η_{KE} that are not as high as those produced by the solid extended cowl, although the improvement over the case without extended solid or virtual cowl is quite substantial. As seen in Table 2, to match the k_m of the solid extended cowl at Mach 6, the power level has to be increased to 35 MW/m and the source moved farther from the body (to be discussed), although an appreciable gas heating makes η_{KE} in this case somewhat lower than that given by the solid cowl.

All computations in this work were performed with $12{,}500 \times 240$ grid. As shown in Table 3, the computed parameters are little different from those computed with a coarser grid, 6250×120.

In all of the calculations described, the energy addition profile was assumed to be circular-cylinder Gaussian heat addition, with $r_{\text{eff},x} = r_{\text{eff},z} = r_{\text{eff}}$. We have also run a series of calculations with elliptical-cylinder Gaussian heating profiles, $r_{\text{eff},x} \neq r_{\text{eff},z}$. Stretching the energy addition profile along the flow, while maintaining constant total power, was found to result in a small improvement in inlet performance. Specifically, as indicated in Table 4, where the optimum elliptical profile cases are compared with the best circular profile case and with the solid extended cowl case, the optimum energy addition profile for this set of condition (Mach number, inlet geometry, and total power) corresponds to $r_{\text{eff},x} = 15 r_{\text{eff},z}$. We further found that slightly tilting the stretched heating profile with respect to x axis can improve the performance. The optimum angle turned out to be $\alpha_q = 2.5$ deg, which, perhaps not coincidentally, equals the angle of the first ramp. Figure 13 shows the optimum

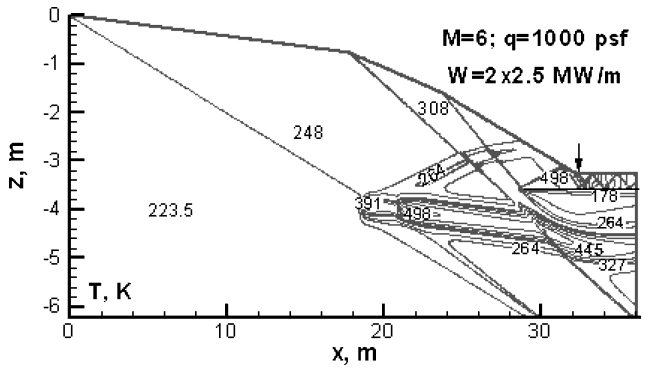

Fig. 12 Static temperature contour lines in Mach 6, 1000-psf case with two optimally located energy addition sources of 2.5 MW/m power each; each source circular Gaussian with $r_{\text{eff}} = 0.2$ m.

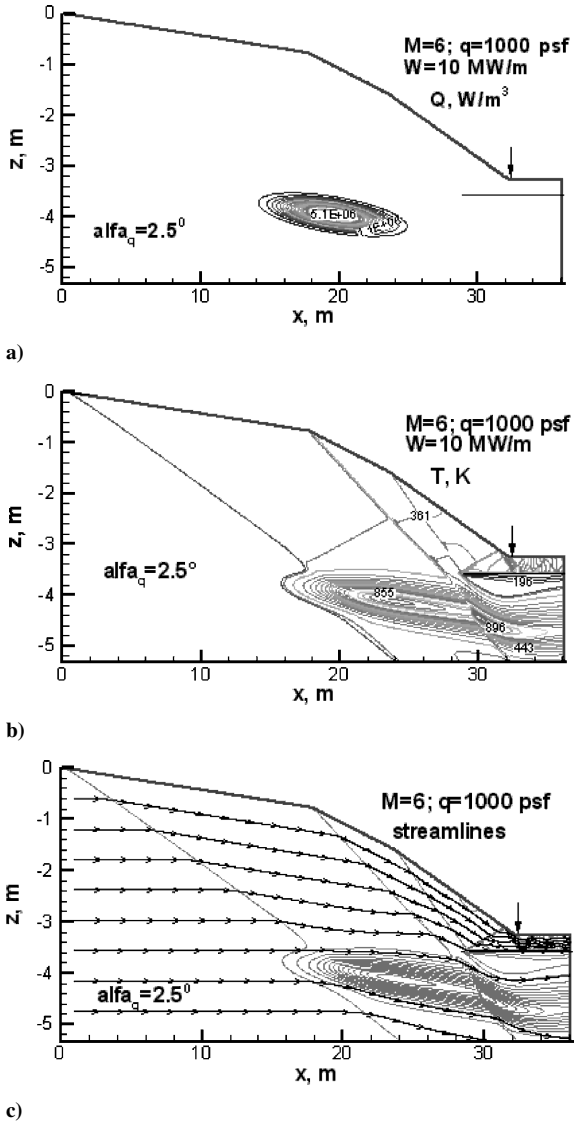

Fig. 13 Mach 6, 1000 psf, with 10-MW/m heating source: a) power density of optimally located, stretched, and tilted 10-MW/m source, b) static temperature contours, and c) flow streamlines.

case with stretched and tilted heating profile at Mach 6. Overall, although stretched and tilted heating profiles do perform better than the circular profiles, the improvement is only incremental.

Finally, the constraint that the energy addition has to be placed at or only slightly below the cowl level was relaxed. For the Mach 6, 1000-psf flight, the circular-cylinder Gaussian heating profile with $r_{\text{eff}} = 0.2$ m and the total power of 5 MW/m was positioned at different vertical locations z below the cowl level z_{cl}. The streamwise coordinate of the center of energy addition region was held constant at $x_Q = 0.5$, 5.5, and 10.5 m. The results are summarized in Fig. 14, and the flowfield in one of the optimum cases is shown in Fig. 15. Freestream conditions shown in Fig. 14 are Mach 6 and 1000 psf. The values of performance parameters in the absence of energy additions are indicated. In each case, the best inlet performance turned out to occur when the shock generated by the energy addition passed through the point of intersection of the nose shock with the upstream

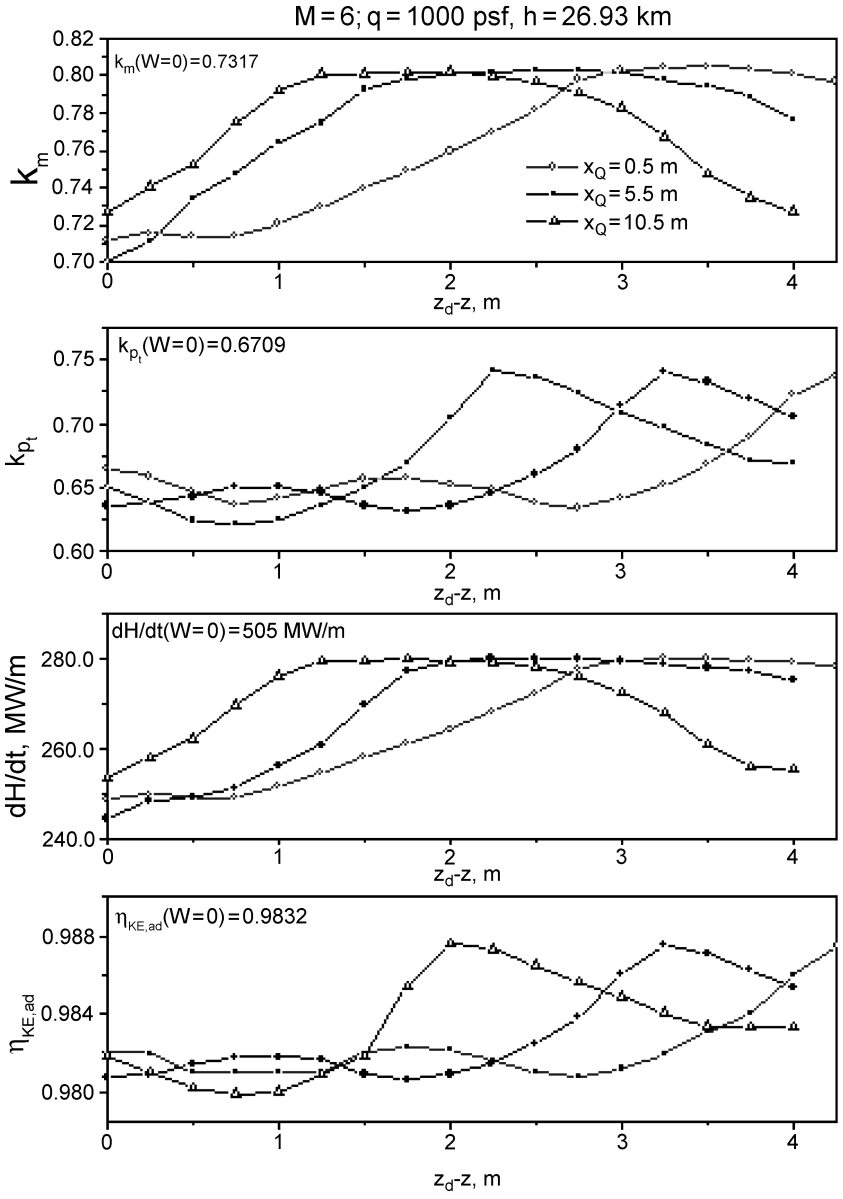

Fig. 14 Inlet performance parameters vs vertical location.

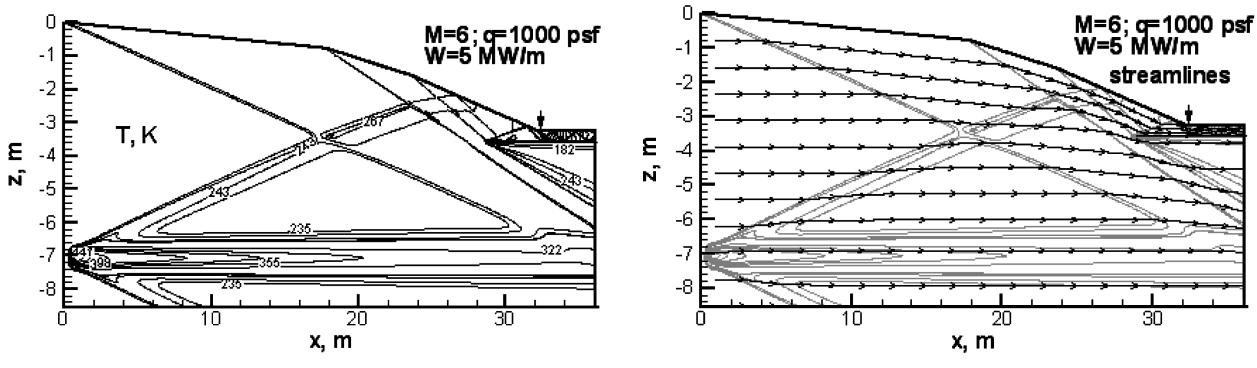

a) b)

Fig. 15 Maximum mass capture k_m case of Fig. 14: a) static temperature contours and b) flow streamlines.

continuation of the cowl line, as expected. The best η_{KE} achieved was equal to, and the best k_m only incrementally superior to, those in the case with energy addition slightly below the cowl level. Given that the performance increase is small, and that it can be practically difficult to implement and control energy addition far from the vehicle surface, it appears advantageous to work with energy addition at or slightly below the cowl level. However, note that, although matching the k_m given by the extended solid cowl at Mach 6 does not seem possible with energy addition concentrated at or just below the cowl line (Table 2), increasing the power of the heating source while moving the source away from the body can yield the k_m equal to that of the solid cowl. Indeed, included in Table 2 are two cases with energy addition centered substantially below the cowl line and with power depositions of 20 and 35 MW/m. As seen in Table 2, the 35-MW/m case does match the k_m of the extended solid cowl, although with somewhat lower η_{KE}. Note that, at power levels as high as 35 MW/m, the optimum location of the energy addition should be farther from the body; thus, the performance shown in Table 2 can be improved on. (The detailed calculations of this case are left for future work.)

IV. Conclusions

The modeling performed in this work demonstrates that a virtual cowl created by energy deposition upstream of the cowl lip can substantially increase mass capture and kinetic energy efficiency of the inlet. The performance of the virtual cowl can approach or match that of a would-be upstream solid extension of the cowl. With the power deposition of only 2–3.5% of the enthalpy flux into the inlet, the mass flow rate entering the inlet can be increased by more than 11%, with no loss of kinetic energy efficiency.

The optimum location of the virtual cowl is such that the shock generated by the energy addition passes through the point where the nose shock intersects with the upstream continuation of the cowl line. Stretching and tilting the energy addition region can improve performance, although incrementally. Energy addition far from the vehicle surface can also improve performance, but only slightly, and the improvement would probably be negated by technical difficulties in depositing and controlling large amounts of energy far from the vehicle surface. Thus, the best location for the virtual cowl appears to be at or slightly below the cowl line.

The physical mechanism of energy addition was not analyzed in this paper. Among possible candidates, hot-air jets or plasma-controlled external combustion can be considered. Plasma methods potentially include initiating and controlling ionization by laser sparks of magnetically guided electron beams and depositing energy by non-self-sustained (subcritical) rf or microwave discharges. Note that some inlet designs contain sidewalls extended upstream of the cowl lip.[1] If the sidewalls are extended far enough, they could be used to carry the hardware (electrodes, wiring, electron guns, magnetic coils, etc.) for plasma methods of generation of virtual cowl.

For a virtual cowl created with plasmas, substantial quantities of electric power are required. If the virtual cowl needs to be created for a short time, energy stored or generated with a separate onboard power unit might be used. Another possibility is to generate electric power by running a magnetohydrodynamic (MHD) generator downstream of the combustor. Whether the increase in engine performance given by virtual cowl (plus other improvements, such an increased lift) would outweigh thrust losses caused by the MHD power extraction should be studied in the future.

Acknowledgments

This work was supported by the Air Force Office of Scientific Research. The authors express their gratitude to David Van Wie of Johns Hopkins University, Applied Physics Laboratory, for valuable advice.

References

[1]Van Wie, D. M., "Scramjet Inlets," *Scramjet Propulsion*, edited by E. T. Curran and S. N. B. Murthy, Vol. 189, Progress in Astronautics and Aeronautics, AIAA, Reston, VA, 2000, Chap. 7, pp. 447–511.

[2]Shneider, M. N., Macheret, S. O., and Miles, R. B., "Nonequilibrium Magnetohydrodynamic Control of Scramjet Inlets," AIAA Paper 2002-2251, May 2002.

[3]Kuranov, A. L., and Sheikin, E. G., "MHD Control on Hypersonic Aircraft Under AJAX Concept: Possibilities of MHD Generator," AIAA Paper 2002-0490, Jan. 2002.

[4]Kopchenov, V., Vatazhin, A., and Gouskov, O., "Estimation of Possibility of Use of MHD Control in Scramjet," AIAA Paper 99-4971, Nov. 1999.

[5]Brichkin, D. I., Kuranov, A. L., and Sheikin, E. G., "The Potentialities of MHD Control for Improving Scramjet Performance," AIAA Paper 99-4969, Nov. 1999.

[6]Bityurin, V. A., Klimov, A. I., Leonov, S. B., Bocharov, A. N., and Lineberry, J. T., "Assessment of a Concept of Advanced Flow/Flight Control for Hypersonic Flights in Atmosphere," AIAA Paper 99-4820, Nov. 1999.

[7]Macheret, S. O., Shneider, M. N., and Miles, R. B., "Magnetohydrodynamic Control of Hypersonic Flow and Scramjet Inlets Using Electron Beam Ionization," *AIAA Journal*, Vol. 40, No. 1, 2002, pp. 74–81.

[8]Macheret, S. O., Shneider, M. N., and Miles, R. B., "Magnetohydrodynamic and Electrohydrodynamic Control of Hypersonic Flows of Weakly Ionized Plasmas," *AIAA Journal*, Vol. 42, No. 7, 2004, pp. 1378–1387; also AIAA Paper 2002-2249, May 2002.

[9]Leonov, S., Bityurin, V., Youriev, A., Savishchenko, N., Pirogov, S., and Ryzhov, E., "Problems in Energetic Method in Drag Reduction and Flow/Flight Control," AIAA Paper 2003-0035, Jan. 2003.

G. Candler
Associate Editor